

See discussions, stats, and author profiles for this publication at: <https://www.researchgate.net/publication/228097058>

# Growth of N,N'-Bis(1-ethylpropyl)perylene-3,4,9,10-tetracarboxdiimide Films on Ag (111)

ARTICLE *in* THE JOURNAL OF PHYSICAL CHEMISTRY C · JUNE 2013

Impact Factor: 4.77 · DOI: 10.1021/jp9051769

---

CITATIONS

11

READS

69

## 11 AUTHORS, INCLUDING:



Hicham Hamoudi

37 PUBLICATIONS 426 CITATIONS

[SEE PROFILE](#)



maria luz Martiarena

National Scientific and Technical Research...

50 PUBLICATIONS 323 CITATIONS

[SEE PROFILE](#)



E.A. Sánchez

Centro Atómico Bariloche

94 PUBLICATIONS 586 CITATIONS

[SEE PROFILE](#)



Luca Pasquali

Università degli Studi di Modena e Reggio ...

101 PUBLICATIONS 1,056 CITATIONS

[SEE PROFILE](#)

## Growth of *N,N'*-Bis(1-ethylpropyl)perylene-3,4,9,10-tetracarboxdiimide Films on Ag (111)

Laura N. Serkovic Loli,<sup>†</sup> Hicham Hamoudi,<sup>‡</sup> J. Esteban Gayone,<sup>†</sup> M. Luz Martiarena,<sup>†</sup> Esteban A. Sánchez,<sup>\*,†</sup> Oscar Grizzi,<sup>†</sup> Luca Pasquali,<sup>§,||</sup> Stefano Nannarone,<sup>§,||</sup> Bryan P. Doyle,<sup>§,||</sup> Céline Dablemont,<sup>‡</sup> and Vladimir A. Esaúlov<sup>‡</sup>

*Centro Atómico Bariloche-Instituto Balseiro-CNEA-UNCuyo-CONICET, 8400 S.C. de Bariloche, Río Negro, Argentina, Laboratoire des Collisions Atomiques et Moléculaires, CNRS-UMR 8625 Université Paris-Sud, 91405 Orsay, France, Dipartimento di Ingegneria dei Materiali e dell'Ambiente, Università di Modena e Reggio Emilia, 41100 Modena, Italy, CNR-INFM Lab. TASC, s.s. 14 km 163.5 in Area Science Park, 34012 Basovizza, Italy*

Received: June 2, 2009; Revised Manuscript Received: August 14, 2009

We have studied the self-assembly characteristics, the electronic structure, and the thermal stability of thin *N,N'*-bis(1-ethylpropyl)perylene-3,4,9,10-tetracarboxdiimide (EP-PTCDI) films grown on Ag (111) by a broad set of surface science analysis techniques. The deposition of single molecules to the formation of very thin films performed at room temperature under ultrahigh-vacuum (UHV) conditions was followed by atomic force microscopy (AFM), scanning tunneling microscopy (STM), ultraviolet photoemission spectroscopy (UPS), X-ray photoemission spectroscopy (XPS), and near edge X-ray absorption fine structure (NEXAFS), and was modeled by density functional theory (DFT) calculations. STM pictures show that substrate step edges are the starting point for molecule adsorption, which is followed by formation of islands and eventually a monolayer. The monolayer is composed of large domains with ordered molecules with their perylene-3,4,9,10-tetracarboxdiimide (PTCDI) core lying almost parallel to the surface. For further exposure, multilayer stacked domains are formed. For thicker films molecular order could not be established. Upon heating it is found that the multilayer is stable up to 150 °C where a rapid desorption takes place, followed by the dissociation of the molecules, leaving an ordered monolayer of presumably perylene core type molecules.

### 1. Introduction

Planar organic molecules have been adsorbed and self-assembled on a variety of substrates such as noble metals, transition metals with incomplete d-shells, and semiconductors. The goal of such studies is the formation of thin and well-ordered semiconducting layers. They give the possibility of controlling molecular deposition in order to generate specific supramolecular surface assemblies.<sup>1</sup> They also present increasing applications in gas sensors,<sup>2</sup> photocatalysis,<sup>3</sup> or optoelectronic devices like light-emitting diodes,<sup>4,5</sup> transistors,<sup>6</sup> and solar cells.<sup>7–9</sup> The necessity of creating new semiconductor layers with different electronic properties, unlike the well-known p-type semiconductor PTCDA (3,4,9,10-perylenetetracarboxylic dianhydride),<sup>10</sup> has encouraged detailed research on new and larger molecules tailored with specific functionalities. In this way, functionalized PTCDI (perylene-3,4,9,10-tetracarboxdiimide) derivative molecules have been shown to be very good candidates for production of n-type semiconductor thin films<sup>11,12</sup> with the possibility of constructing different optoelectronic devices.<sup>8,13–16</sup> However, critical design parameters in electronic devices,<sup>14,17</sup> i.e., order, anisotropic properties, and thermal stability of the layers, can be impaired or changed because the interactions among those molecules and between them and the

substrate have a high degree of complexity.<sup>18–20</sup> Therefore more detailed investigations of differently functionalized molecules, such as PTCDI, are necessary to obtain information on their electronic and crystallographic properties by using different complementary analysis techniques.

In a previous work<sup>21</sup> we started to study the growth of *N,N'*-bis(1-ethylpropyl)perylene-3,4,9,10-tetracarboxdiimide (EP-PTCDI) films, under ultrahigh-vacuum (UHV) conditions, by scanning tunneling microscopy (STM) and time of flight-direct recoil spectroscopy (TOF-DRS). Our interest in this molecule stems from some experiments where its use for molecular electronic applications<sup>14,22</sup> was proposed, but the characteristics of layer formation were unknown. In particular it was interesting to find out how the EP (ethylpropyl) end groups might affect order, taking into account that the mobility of the molecules on the surface and the lateral intermolecular interaction can be reduced by the presence of the end groups as it was observed for DiMethyl-PTCDI (DiMe-PTCDI) molecules.<sup>17,18</sup>

In this paper we report experiments and calculations involving several complementary techniques to provide an overview of the film characteristics during growth and desorption processes. Information relevant to the molecular order and details of the electronic structure at different stages of the multilayer growth and thermal desorption have been provided by STM measurements and ultraviolet photoemission spectroscopy (UPS). X-ray photoelectron spectroscopy (XPS) gives indications on composition and chemical effects. Near edge X-ray adsorption fine structure (NEXAFS) is used to study order in the film. Density functional theory (DFT) calculations allow the study of the

\* To whom correspondence should be addressed. Phone: +54 2944 445234. Fax: +54 2944 445299. E-mail: esanchez@cab.cnea.gov.ar.

<sup>†</sup> CAB-IB-CNEA-UNCuyo-CONICET.

<sup>‡</sup> CNRS-UMR 8625 Université Paris-Sud 8625.

<sup>§</sup> Università di Modena e Reggio Emilia.

<sup>||</sup> CNR-INFM Lab. TASC.

<sup>¶</sup> Current address: Department of Physics, University of Johannesburg, P.O. Box 524, Auckland Park 2006, South Africa.

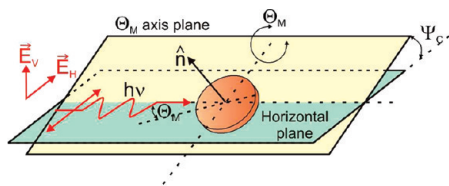


**Figure 1.** NEXAFS experimental geometry. The electric field vector of the elliptically polarized X-rays has two components  $E_H$  (major) and  $E_V$ .  $\Theta_M$  is the incidence angle of the light with respect to the sample surface plane;  $\Psi_C$  is the sample rotational angle around the beam axis; and  $\hat{n}$  is the surface normal.

geometrical configuration and the electronic properties of a single molecule in vacuum and of the monolayer adsorbed on the surface.

In this work we chose the Ag (111) substrate, because its interaction with the adsorbate is not so strong, as in the case of silicon<sup>23,24</sup> where no order has been found in the first monolayer even at high substrate temperatures, and it allows the formation of self-assembled monolayers as has been observed in the case of PTCDA,<sup>9,25–28</sup> PTCDI, and a few other simple PTCDI derivatives.<sup>19,20,17,29</sup>

The stability of the organic layers up to temperatures higher than room temperature is essential for electronic applications where the temperature range preferred for device fabrication is from 50 to 150 °C. However, there are few systematic studies performed on such systems, and they usually correspond to temperatures well below desorption.<sup>14,17,19,28</sup> Therefore, here besides measurements on adsorption at room temperature we also performed measurements for desorption in the range of 20 to 450 °C.

## 2. Experimental and Theoretical Method

**2.1. Experiment.** The XPS, UPS, and NEXAFS measurements were performed at the BEAR bending magnet beamline<sup>30</sup> at the Elettra synchrotron in Trieste (Italy). The AFM and STM measurements and DFT calculations were performed at the Centro Atómico Bariloche (Argentina). In the following we briefly describe the setups.

Photoemission measurements were carried out for the substrate (Ag 3d) and overlayer (C 1s, O 1s, and N 1s) core levels and for the valence band. Experiments were performed at normal emission, at 45° of p-polarized light incidence angle, and with a hemispherical deflection analyzer (66 mm mean radius) driven at constant pass energy, with 300 meV electron energy resolution. The valence band was measured with a photon energy of 30 eV. Concerning the core levels, the photon energy ( $h\nu = 450$  eV for Ag 3d,  $h\nu = 385$  eV for C 1s,  $h\nu = 600$  eV for O 1s, and  $h\nu = 450$  eV for N 1s) was chosen in order to measure the photoelectron peaks of the different core levels approximately at kinetic energies  $\leq 100$  eV. Such a condition was pursued in order to maximize the surface sensitivity, measuring photoelectrons with kinetic energies corresponding to the minimum of the inelastic mean free path ( $\Lambda \approx 0.6$  nm).<sup>31,32</sup> Moreover, the use of lower photon energies with respect to the Al and Mg K $\alpha$  lines routinely available in conventional laboratory XPS sources results in a higher photoabsorption cross section<sup>33</sup> for the different core levels of interest.

The NEXAFS at the C 1s edge was measured by using the experimental geometry shown in Figure 1. To measure linear dichroism effects, the incidence angle of the light with respect to the sample surface plane ( $\Theta_M$ ) was kept fixed at 10°, and the sample was then rotated around the beam axis by an angle  $\Psi_C$ , from  $\Psi_C = 0^\circ$  (s-scattering condition) to  $90^\circ$  (p-scattering

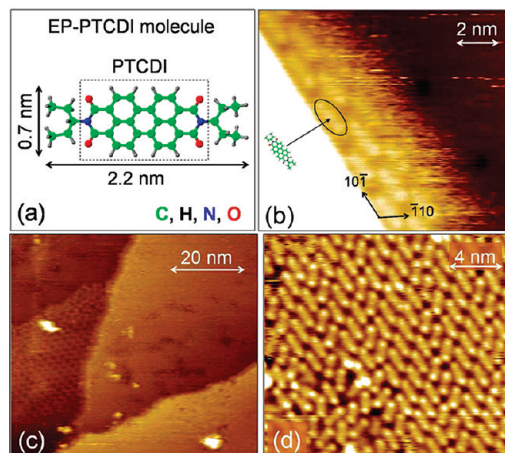


**Figure 2.** Adsorption of EP-PTCDI molecules for a submonolayer coverage. (a) Sketch of a single molecule. (b) STM image of a monatomic Ag step where the molecules start to self-assemble. Panels c and d show the formation of islands with ordered molecule domains. The images were acquired with +3 V sample polarization bias voltage and 50 pA tunneling current.

condition). This guarantees that the illuminated area remains virtually unchanged for different  $\Psi_C$  angles, and that the incidence angle is unchanged. The synchrotron beam was elliptically polarized with its major electric field component oriented in the horizontal direction H, giving a polarization factor  $P = |\vec{E}_V|^2 / (|\vec{E}_V|^2 + |\vec{E}_H|^2)$  of 0.29–0.33, or equivalently, an ellipticity  $\epsilon = |\vec{E}_V|^2 / |\vec{E}_H|^2$  of 0.4–0.5. These values were chosen as a good compromise to distinguish dichroism effects without reducing the beam flux. Measurements were carried out by acquiring the drain current from the sample (total yield mode). Photon energy resolution was set at 0.1 eV. To take into account the incident flux decay and the beam fluctuation and to correct for its dependence on wavelength (source plus optics transmission), the absorption spectra were first normalized to the current drained by a gold mesh (flux monitor) and to a reference absorption spectrum taken under the same experimental conditions and energy range on a carbon free Ag (111) surface. After that, the spectra were normalized in order that they coincide for photon energies far below and far above the edge region. This is equivalent to normalizing the signal to the number of sampled C atoms. Characteristic features of the flux monitor signals were used for the alignment of the energy scales of the spectra. Reproducibility was tested by taking multiple scans. All measurements were performed at room temperature.

In Bariloche the measurements were carried out on a setup with a variable temperature STM and a low energy electron diffraction (LEED) system (both from Omicron Nanotechnology). The AFM images were taken by an Autoprobe CP from Park Scientific Instruments working in air.

The Ag (111) sample was obtained from MaTecK GmbH<sup>34</sup> as a single crystal disk (10 mm diameter, 2 mm thick, hat shape with a hole for a thermocouple) of 99.999% purity, oriented to within  $<0.4^\circ$ . The surface was cleaned in the ultrahigh vacuum chamber by cycles of Ar sputtering and annealing to 450 °C. The surface initial condition was checked by LEED and STM in Bariloche and by XPS at Elettra.

The organic molecule *N,N'*-bis(1-ethylpropyl)perylene-3,4,9,10-tetracarboxdiimide (EP-PTCDI, also named as 2,9-di(pent-3-yl)anthra[2,1,9-def:6,5,10-d'e'f']diisoquinoline-1,3,8,10-tetraone, Catalogue No. ST 1/23) was synthesized and provided by Sensient Imaging Technologies GmbH<sup>35</sup> as a red powder. A sketch of the molecule is shown in Figure 2a.

The adsorption of EP-PTCDI molecules was carried out by evaporating the molecules from a thoroughly degassed Knudsen cell. During the whole evaporation process the pressure was kept below  $10^{-9}$  Torr.

**2.2. Theory.** We have carried out DFT calculations within the slab-supercell approach<sup>36</sup> by using the ab initio total energy and molecular dynamics program VASP (Vienna ab initio simulation program).<sup>37</sup> The one-electron Kohn–Sham orbitals are developed by using a plane-wave basis set, while electron–ion interactions are described through the ultrasoft pseudopotentials (USSPs).<sup>38,39</sup> Exchange and correlation (XC) is described within the generalized gradient approximation (GGA) introduced by Perdew and Wang (PW91).<sup>40</sup> The sampling of the Brillouin zone is carried out according to the Monkhorst–Pack method.<sup>41</sup> Electron smearing,  $\sigma$ , was introduced following the Methfessel–Paxton technique<sup>42</sup> with  $\sigma = 0.2$  eV and all the energies are extrapolated to 0 K. The cutoff energy was 350 eV and the calculations were spin restricted. To obtain the single molecule geometrical parameters we performed a full atoms coordinates relaxation in a unit cell of  $3.10 \times 2.20 \text{ nm}^2$  and a vacuum layer with thickness of 2.90 nm using a  $1 \times 1 \times 1$   $k$ -point mesh.

The monolayer of EP-PTCDI molecules adsorbed onto a Ag (111) surface was described considering a unit cell with lattice parameters  $a_1 = (2.65, 0.0, 0.0)$  nm and  $a_2 = (-1.03, 0.76, 0.0)$  nm, using a  $3 \times 3 \times 1$   $k$ -point mesh. The vacuum layer region between consecutive slabs is  $\sim 4.24$  nm, thick enough to ensure negligible interactions between periodic images normal to the surface when we include the molecule. The choice of  $a_1$  and  $a_2$  is justified in the next section. The theoretical lattice constant obtained for the Ag single crystal by using a  $15 \times 15 \times 15$   $k$ -point mesh was  $a_{\text{calc}} = 0.4171$  nm, in good agreement with the experimental value,  $a_{\text{exp}} = 0.4078$  nm. No significant relaxation of the interlayer distance with respect to the Ag bulk value was observed.

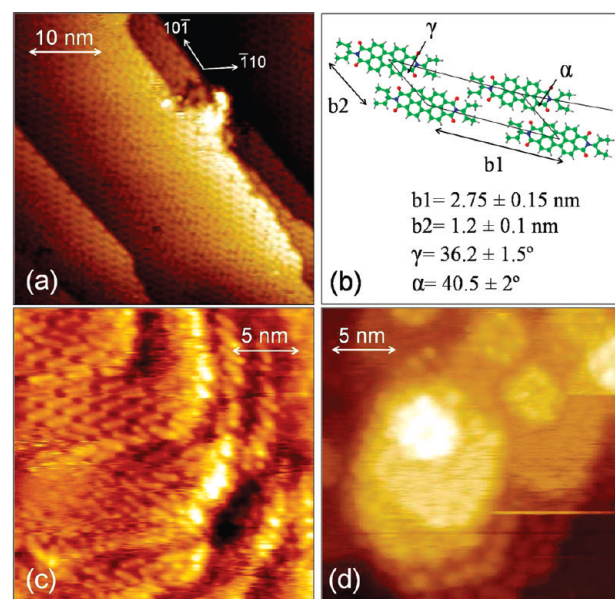
### 3. Results and Discussion

**3.1. EP-PTCDI Adsorption. 3.1.1. STM Measurements and Theoretical Modeling.** *Monolayer Growth.* Panels b–d of Figure 2 show STM images corresponding to the first steps of the adsorption. The images in the submonolayer regime (less than 0.3 ML) show that the self-assembly process begins on step edges which are aligned along the silver [101] or [110] main surface directions. At this low coverage, the PTCDI core of the molecules is found to lie flat over the substrate and is oriented almost parallel to these directions. Under the optimized STM experimental conditions necessary to get good molecular resolution, i.e., high bias voltages (+2 to +4 V) and very low tunnel currents ( $\sim 50$  pA), the Ag substrate atoms cannot be seen because the tip is far from the Ag atoms. This precludes the determination of the adsorption site of the organic molecules with respect to the substrate atom position.

At higher exposures, but still less than one monolayer, islands start to develop away from the steps. In panel d of Figure 2 we can see the beginning of the self-assembly process by zooming part of the island shown on Figure 2c. Other derivative PTCDI molecules with shorter alkane end groups (DiMe-PBDCI) grown on Ag (111) display such a behavior.<sup>18</sup>

The height profile measured for the first row of molecules and for small islands formed next to a step indicates an apparent height (the height given by the STM at constant current measurement mode) of 0.11–0.15 nm, lower than the monatomic step height of Ag (111) (0.239 nm).

If we increase the exposure the EP-PTCDI molecules form a self-assembled monolayer with the Ag surface fully covered.



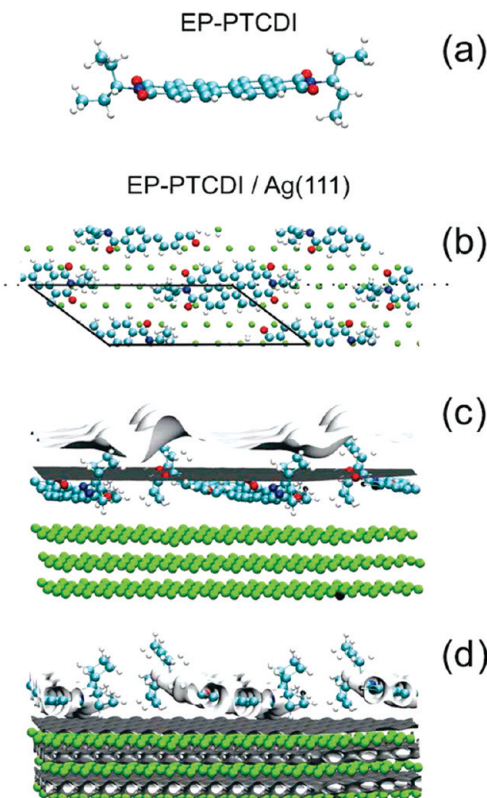
**Figure 3.** STM images corresponding to the formation of (a) a fully covered self-assembled monolayer of EP-PTCDI molecules (+2.5 V; 50 pA) and (c, d) the growth of 3D islands for much higher exposures, about 4 ML (+3 V; 50 pA). Panel b shows the unit cell structure obtained for the monolayer.

Figure 3a shows a STM image of the ordered monolayer. By analyzing several images at this coverage we have seen that the molecules still remain with the PTCDI core lying flat on the surface with a structure mainly described by the unit cell shown in panel b of Figure 3.

The adsorption kinetics starting with single molecule adsorption to the formation of several layers was studied in a previous work<sup>21</sup> by TOF-DRS. In these measurements we observed that the growth up to 1 ML was linear, thus indicating that the sticking coefficient, i.e., the ratio of the number of molecules that do adsorb on a surface to the total number of molecules that impinge upon that surface, was constant up to the completion of the first monolayer. Combining these results with the STM observations we concluded that the growth rate was constant, without favoring the formation of 3D islands until the completion of the first monolayer. For coverages higher than one monolayer it was difficult to obtain this information with TOF-DRS.

The geometrical results of the DFT calculations performed for the isolated single EP-PTCDI molecule and the assembly of a monolayer on Ag (111) are shown in Figure 4. Starting from the initial geometrical configuration described in the sketch of Figure 2a, the relaxation of the coordinates of all atoms was calculated. The optimized configuration is shown in Figure 4a, where it can be observed that the molecule is no longer fully flat: both EP end groups are rotated with respect to the PTCDI core plane and the core itself is slightly bent.

To perform the calculation for the adsorption of a monolayer of EP-PTCDI on Ag (111) we used, as the initial configuration, the optimized geometrical parameters of the single molecule and stacked it on a three-layer slab to represent the Ag (111) surface. To carry out the DFT calculation within the slab-supercell approach we need to commensurate the unit cell with the Ag (111) substrate. To work with the smallest amount of Ag atoms we choose a unit cell with  $|a_1| = 2.65$  nm,  $|a_2| = 1.28$  nm, and  $\gamma = 36.2^\circ$ , which is very close (within experimental error) to that deduced from STM images (Figure 3b). We allow the relaxation of every atomic coordinate of the



**Figure 4.** Results of DFT calculations. (a) Optimized geometrical configuration of an isolated single EP-PTCDI molecule; top (b) and side (c, d) views of the optimized geometrical configuration of a monolayer of EP-PTCDI grown on Ag (111). Partial charge isodensity of EP-PTCDI/Ag (111) (light gray) and clean Ag (111) (dark gray). Isovalues: (c)  $2 \times 10^{-5}$  states/volume and (d)  $4 \times 10^{-2}$  states/volume (see text).

molecule and the two topmost layers of Ag (111). The top view of the optimized configuration is shown in panel b of Figure 4. The monolayer arrangement remains entirely over the silver surface, and the EP end groups shift upward and stay rotated with respect to the PTCDI core, which continues to bend and forms an angle of about  $6^\circ$  with respect to the surface plane. No significant relaxation of Ag atoms was observed.

Panels c and d of Figure 4 show the partial charge density (PARCHG) evaluated within an electronic band energy range between the Ag (111) Fermi energy and +3 eV. In the Tersoff–Hamann approach,<sup>43</sup> this partial charge density describes the STM images when the bias voltage is +3 V and the isodensity value ( $n(I) [\text{A}^{-3}]$ ) is proportional to the fixed current in constant current mode STM experiments ( $I [\text{nA}]$ ).<sup>44</sup> In these panels we present two extreme cases of isodensity values: (Figure 4c)  $2 \times 10^{-5}$  and (Figure 4d)  $4 \times 10^{-2}$  states/(unit cell volume), which represent low and high constant current STM measurements. In both panels, the light gray curves correspond to the isodensity surface of EP-PTCDI/Ag (111) and the dark ones to the Ag (111) (same slab without the molecule).

Figure 4d shows that when the isodensity value is high, corresponding to a high STM current, it is possible to observe the electronic corrugation of the metal surface. Besides, the isodensity curve does not completely surround the molecule. These results would explain why in the high constant current mode it was very difficult to obtain STM images showing at the same time the bulk atoms and the entire molecule. The absence of high charge density around the end groups would cause the tip to crash on it, affecting the molecule organization or modifying the tip itself. On the other hand, when the iso-

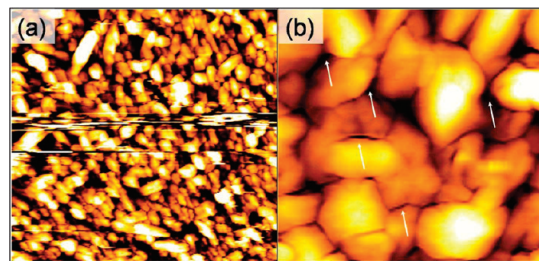


**Figure 5.** AFM images of a  $\sim 20$  nm thick EP-PTCDI film: (a)  $4 \times 4 \mu\text{m}^2$  and (b)  $1 \times 1 \mu\text{m}^2$ . White arrows in panel b indicate some regions where the structures did not coalesce.

is low enough the isodensity curve completely surrounds the molecule, so it is possible to observe the entire EP-PTCDI molecule (Figure 4c) but one loses the electronic corrugation coming from Ag atoms.

Note that in panel c of Figure 4 the higher heights in the isodensity curve correspond to the rotated EP end groups. These maxima explain the bright points observed at the end of the EP-PTCDI molecules in the STM images (Figure 2d).

Since the STM images were acquired at constant current mode, the apparent height of the adsorbed molecule with respect to the surface can be calculated from the normal distance between the EP-PTCDI/Ag (111) and the clean Ag (111) isodensity curves. The isodensity curve for the clean Ag (111) surface (Figure 4c) moves out of the surface farther than the EP-PTCDI/Ag (111) isodensity curve (for the same very low isodensity value). This leads to an apparent height that is lower than the real distance between the molecule and surface atoms. Even though the calculated apparent height was higher than the experimental one, this result can partially explain this trend.

**Multilayer Growth.** If we continue to increase the exposure to 4 ML, we start to see the growing of 3D island structures formed by a few ordered layers of EP-PTCDI (see Figure 3c,d). These islands show a less ordered surface with an interlayer spacing of  $\sim 0.26$  nm. They have a higher interlayer spacing compared to the apparent height of the small monatomic islands or of the molecules next to a step. This change indicates that the interaction among the molecules could be weaker than that with the metallic substrate, as has been proposed for different perylene functionalized molecules.<sup>17,28</sup> The STM image size of single molecules and their ordering at  $\sim 4$  ML looks similar to that in the first ML, suggesting that the molecules are stacking with their PTCDI cores parallel in consecutive layers and maintaining their crystallographic order.

STM images were difficult to obtain for thicker films so we used atomic force microscopy (AFM) working in air. In Figure 5 we show two AFM images of  $4 \times 4$  and  $1 \times 1 \mu\text{m}^2$  obtained after growing an EP-PTCDI film of about 20 nm thick. It is clearly observed from these figures that 3D structures continue to be formed for thicker films. The topography of the surface is formed by grains or islands of about 160 to 240 nm in diameter with a roughness (root-mean-square deviation of the height distribution) of about 15 nm. We have also observed from the height profile analysis of the images that there are small regions on the film where these structures do not completely coalesce. Some of these regions were indicated by white arrows on Figure 5b. The molecular order of these islands could not be obtained by the AFM.

**3.1.2. Valence Band Measurements.** Valence band spectra taken with p-polarized 30 eV photons are shown in Figure 6. In the left panel the extended spectra are reported, including the region where the Ag 4d band is giving contributions. In the

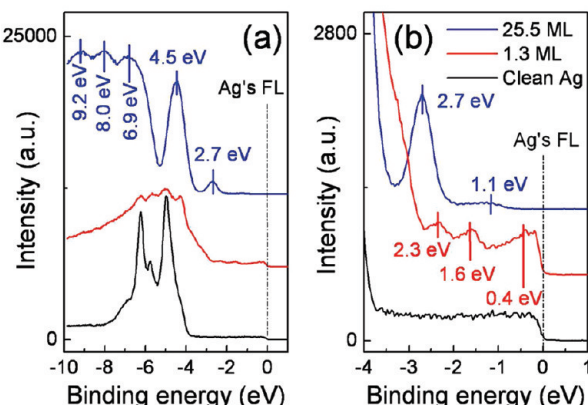


**Figure 6.** Valence band spectra of 0, 1.3, and 25.5 ML of EP-PTCDI evaporated on Ag (111). Panel b shows a spanned region around the Fermi level (FL).

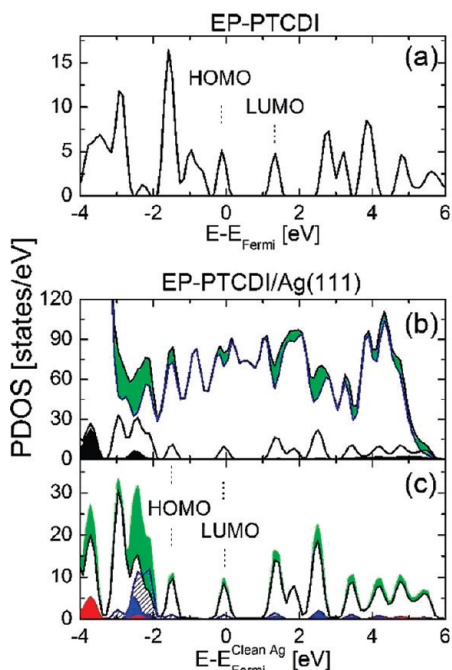


**Figure 7.** Projected density of states (PDOS) for (a) an isolated single EP-PTCDI molecule and (b, c) a monolayer of EP-PTCDI on Ag (111). In panel b the green area indicates the difference between the total and Ag PDOS. The black curve and black shaded area are the contributions to the PDOS coming from the entire molecule and just its EP end groups, respectively. In panel c each colored line corresponds to the contributions of each atom to the PDOS of the adsorbed molecule: green, total molecule; black, carbon; red, hydrogen; blue, nitrogen; and blue diagonal pattern, oxygen.

right panel, a higher magnification of the region just below the Fermi level (FL) is presented. The spectrum of the clean Ag (111) surface is also shown for comparison (lower curve).

For about 1 ML coverage, we observe a modification of the valence band spectrum with the appearance of new features in the region just below the Ag FL. Similar structures have already been observed for PTCDA adsorption of Au, Ag, and Cu<sup>45,46</sup> and for PTCDI and DiMe-PTCDI deposition on S-passivated GaAs (100).<sup>47</sup>

To account for the observed structures a DFT calculation of the total projected density of states (PDOS) has been performed. The results are shown in Figure 7 where panel a corresponds to the single isolated molecule and panel b and c to the monolayer of EP-PTCDI molecules arranged on Ag

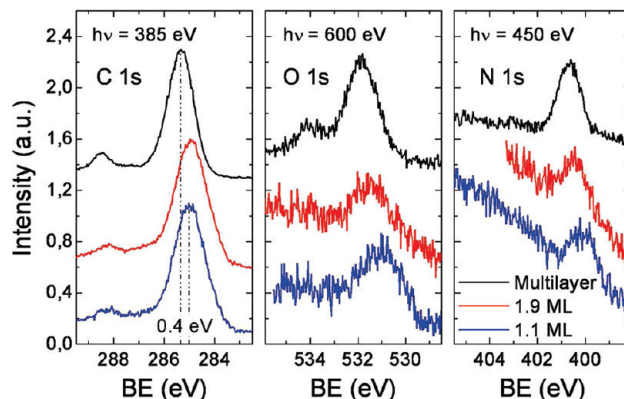


**Figure 8.** C 1s, O 1s, and N 1s XPS spectra measured for 1.1, 1.9, and 20 layers of EP-PTCDI deposited on Ag (111).

(111). We observe that when the molecule is adsorbed on Ag (111) the electronic states of the single molecule shift to lower energies with respect to the clean Ag (111) Fermi energy.

For 1 ML coverage, the first structure at  $-0.4$  eV of binding energy can be associated with a partial filling of the LUMO molecular state, with electrons coming mainly from C atoms of the PTCDI core (Figure 7c). The structure at  $-1.6$  eV and the broadening observed in the Ag 4d band (for energies around  $-3$  eV) are also due to core PTCDI C electrons.

On the other hand, Figure 7c shows that the structure at  $-2.3$  eV is formed by electronic states coming from N, O, and C atoms of the PTCDI core and the EP end groups.

For the multilayer spectrum, which corresponds to approximately 25 ML, the neutral HOMO state shifts to higher binding energy (at  $-2.7$  eV), in agreement with literature reports.<sup>45</sup> This can be explained in terms of a reduced screening of the photoemission hole by the substrate. The HOMO orbital has a  $\pi$  character and is mainly located on the perylene core.<sup>45</sup> For multilayers of DiMe-PTCDI<sup>45</sup> and PTCDA,<sup>46</sup> similar corresponding binding energies have been observed. Thus for these perylene systems and for thick EP-PTCDI films a similar transport gap should be expected.

The Ag 4d band (left panel) is severely damped and modified already at 1 ML of coverage and it is completely obscured at 25.5 ML. Apart from the HOMO state at  $-2.7$  eV, the spectrum displays peaks at  $-4.5$  eV and above, which are attributed to more highly bound states in the molecular film not perturbed by the substrate.<sup>46</sup> A strong attenuation of the photoemission intensity near and below the Ag FL is also observed.

**3.1.3. XPS Measurements.** Figure 8 shows the C 1s, O 1s, and N 1s XPS spectra for different coverages (1.1, 1.9, and 20 ML). The spectra were acquired at normal emission in p-light scattering geometry. The three multilayer spectra are very similar to the ones of a related molecule (DiMe-PTCDI) adsorbed on Ag (111).<sup>17</sup> The line shape is also very similar to that presented by PTCDA adsorbed at metal surfaces.<sup>46</sup> The C 1s spectrum shows a main structure centered at 285.4 eV, formed by contributions from the C atoms of the perylene core, and a small structure at 288.5 eV. While the principal structure is associated to the C atoms in aromatic environment and in the EP tails, the smaller high binding energy feature is ascribed to the carboxylic carbon atoms of the imide group. In spite of the bad signal-to-noise ratio, the O 1s spectrum presents a main structure at 531.9 eV and a small shoulder at around 534 eV, which is associated to the shake up satellite of the main feature.<sup>17,46</sup> Finally, the N 1s spectrum presents a peak at 400.7 eV. No well-resolved

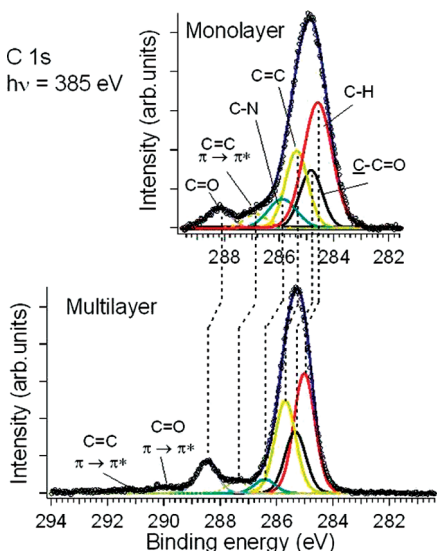


**Figure 9.** Results of the peak fit analysis of the C 1s XPS spectrum of an EP-PTCDI thin film.

satellite is observed in this case (probably due to the feeble intensity and hence poorer statistics).<sup>17</sup>

At low coverages, the C 1s peak is broadened and shifted to lower binding energies. From Figure 8 it can be seen that these two effects are more pronounced the lower the coverage. The rigid shift has to be principally associated to a higher screening of the core hole final state from the substrate metal electrons.

In spite of the high noise signal, the spectra corresponding to low coverages in case of N 1s and O 1s confirm the trend observed for C 1s, as expected for a flat lying configuration where all the molecular groups interact to some extent with the substrate.

To get more specific information, we fitted the C 1s spectra of the mono- and multilayer following the work by Zahn et al.<sup>17</sup> and the results are presented in Figure 9. Each spectrum was decomposed into single Voigt peaks, each peak being characterized by the same Lorentzian width  $W_L = 75$  meV and a Gaussian broadening of  $W_G = 800$  meV.

The main structure of the multilayer spectrum was fitted with four components. The lower binding energy one, at 285 eV, is associated to C atoms bonded to H, either in the perylene core or in the EP groups; the second component at 285.4 is related to the C atoms involved in the C=C=O bonds; the third component at 285.7 eV is related to the C atoms in the center of the perylene part, characterized by C=C bonding; and the fourth component at 286.4 eV is associated to the C atoms bonding to N in C-N bonds. A separate structure at 288.5 eV is associated to the C atoms in the C=O groups. Additional structures are present at 287.4, 290, and 291.4 eV, which can be assigned to multielectron excitations (shake up satellites) associated to  $\pi \rightarrow \pi^*_{C=C}$ ,  $\pi \rightarrow \pi^*_{C=O}$ , and  $\pi \rightarrow \pi^*_{C=C}$  transitions, according to ref 17.

The same peak components were used to fit the spectrum taken at monolayer coverage, as reported in the top panel of Figure 9. It can be seen that all the components present a shift toward lower binding energies, accompanied by an overall broadening. As explained above, this can be mainly justified in terms of the enhanced screening of the C 1s core holes by the substrate electrons, related to a redistribution of charges within the molecule or to charge transfers between the metal and the functional end groups of the molecule. The persistence of the shake up satellites indicates that the aromatic nature of the molecule is preserved in the adsorption.

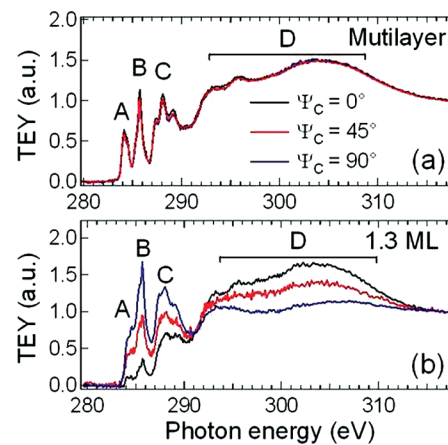


**Figure 10.** C 1s NEXAFS spectra taken at  $\Psi_C$  equal to 0 (s-polarized) and  $45^\circ$  and  $90^\circ$  (p-polarized) for about a monolayer (1.3 ML) and a multilayer (24.2 ML) of EP-PTCDI on Ag (111).

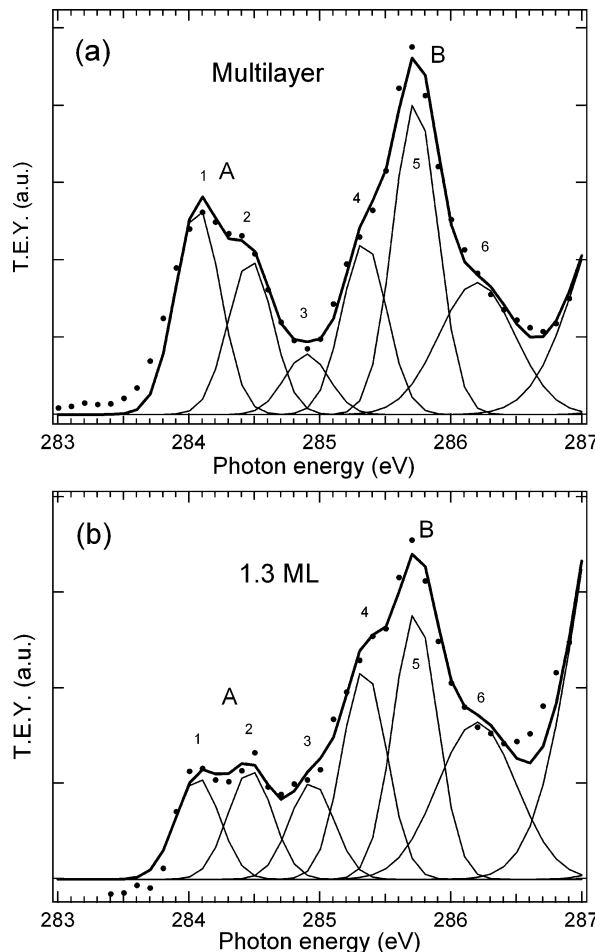


**Figure 11.** Spanned region of features A and B of Figure 10.

**3.1.4. NEXAFS Measurements.** Results of the NEXAFS measurements taken at the C 1s edge are summarized in Figures 10 and 11. Low and high coverage spectra present a series of multiple structures that have been labeled from A to D. Comparing with related systems,<sup>46,48–51</sup> feature A is associated to  $\pi^*$  transitions from the C 1s atoms in the perylene core of the molecule to the LUMO state, feature B to  $\pi^*$  transitions from the same atoms to the LUMO+1 and higher states, and the C multiplet to transitions from the imide and from the ethylpropyl end groups to the LUMO and next higher orbitals.

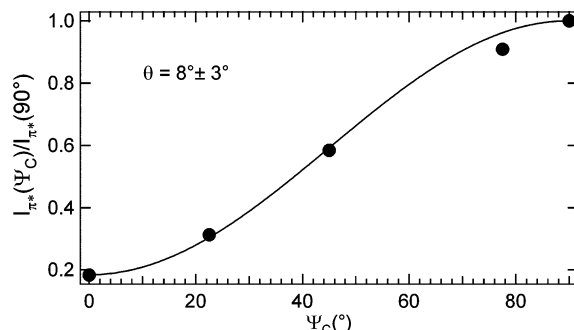


**Figure 12.**  $\pi^*$  intensity measured at different  $\Psi_C$  angles and normalized to the intensity of the  $\pi^*$  transitions at  $\Psi_C = 90^\circ$ .

The broad structures at higher photon energy, indicated by the label D, are associated to  $\sigma^*$ -type transitions from carbon atoms in the aromatic rings and in the EP end groups.

A decomposition of the A and B features into single peaks is shown in Figure 11 for the two coverages with  $\Psi_C = 0^\circ$ , corresponding to s-scattering conditions. Analogous results were obtained for PTCDA<sup>50</sup> and other related molecules with extended  $\pi$ -conjugated ring systems,<sup>48</sup> with the different components labeled from 1 to 6 being associated to  $\pi^*$ -transitions from the different atoms in the molecular central aromatic part. It can be seen both from Figures 10 and 11 that feature A is severely damped at low coverage with respect to the multilayer case. This can be related to the partial filling of the LUMO state at low coverage, as discussed above in relation to the appearance of an additional feature just below the FL in valence band photoemission. Filling of the LUMO would result in a reduced oscillator strength for feature A, which is associated to transitions to this empty state. This effect has already been observed and discussed for PTCDA deposition on Ag<sup>46,49</sup> and for perylene deposition on Cu,<sup>51</sup> which resulted in major modifications of the line shape. In the present case, only an attenuation effect is observed, which can be associated to a weaker chemical interaction between the perylene core of the molecule and the substrate, most likely due to the presence of the EP end groups.

Regarding the angular dependence of the spectra, two distinct behaviors are observed at low and high coverage. At low coverage a clear linear dichroism effect is detected (Figure 10b) while angular effects disappear progressively as the film thickness increases (intermediate coverages are not shown here, only the multilayer case is reported in Figure 10a).

At monolayer coverage the angular dependence suggests a flat lying configuration of the PTCDI core of the EP-PTCDI molecules.  $\pi^*$  related transitions have their dipole moment oriented perpendicular to the molecular plane, and show maximum intensity when the electric field vector is oriented parallel to it. This occurs in the present case at  $\Psi_C = 90^\circ$  (p-light scattering). The opposite takes place for  $\sigma^*$  transitions, which have dipole moments within the molecular plane.

To estimate the average orientation of the molecular plane with respect to the surface plane at low coverage (1.3 ML), we monitored the angular dependence of the  $\pi^*$  resonances (both A and B features). In Figure 12 we show the behavior of the  $\pi^*$  intensity (sum of all features contributing to A and B) measured at different  $\Psi_C$  angles and normalized to the intensity of the  $\pi^*$  transitions at  $\Psi_C = 90^\circ$ .

For ternary symmetry surfaces (111 surfaces with possibly three domains) the intensities can be fitted with the following

relation

$$\frac{I_{\pi^*}(\theta)}{I_{\pi^*}(90^\circ)} = \frac{A\pi(\sin^2 \theta_M \sin^2 \theta + \cos^2 \theta_M \cos^2 \theta) + B\pi \sin^2 \theta}{A_{(\Psi_C=90^\circ)}\pi(\sin^2 \theta_M \sin^2 \theta + \cos^2 \theta_M \cos^2 \theta) + B_{(\Psi_C=90^\circ)}\pi \sin^2 \theta} \quad (1)$$

where  $\theta_M$  is the grazing incidence angle ( $10^\circ$  in our case),  $\theta$  is the tilt molecular angle (to be determined), and

$$\begin{aligned} A &= \varepsilon^2 \cos^2 \Psi_C + \sin^2 \Psi_C - 2\varepsilon \cos \Psi_C \sin \Psi_C \cos \delta \\ B &= \cos^2 \Psi_C + \varepsilon^2 \sin^2 \Psi_C + 2\varepsilon \cos \Psi_C \sin \Psi_C \cos \delta \end{aligned} \quad (2)$$

with  $\delta$  being the phase difference between the vertical and horizontal components of the electric field vector ( $90^\circ$  in our case) and  $\varepsilon$  the photon ellipticity. Both the tilt angle and the photon ellipticity were left as free fit parameters. The best fit result indicates a photon ellipticity of 0.42, which is compatible with the beamline polarization setting and an average tilt of the molecular plane of  $8(\pm 3)^\circ$  with respect to the surface, in agreement with the results obtained by DFT calculations (section 3.1.1). Similar deviations from the perfectly planar configuration were obtained for perylene adsorption on Cu<sup>51</sup> and for PTCDA on Ag,<sup>49</sup> and were attributed to molecular distortions occurring because of chemisorption, possibly involving a bending of the CH-bonds out of the molecular plane.

As far as more layers being deposited on the substrate, we observed a progressive reduction of the linear dichroism dependence. In the multilayer spectrum, where the contributions from the buried interface layer can be considered as negligible, no sizable angular variation was detected. This finding can be attributed (i) to a disordered film, (ii) to an alternate orientation of the molecules, passing from parallel to perpendicular orientation with respect to the substrate plane in adjacent layers, or (iii) to a particular average orientation of the molecular film close to the angle of  $54.7^\circ$ , for which dichroism effects are smeared out.<sup>52</sup> At present we are not able to discriminate between these possibilities from NEXAFS data alone. A flat lying configuration was observed with STM only for low coverage, but 3D islands were seen to develop at higher coverage, where it was not possible to identify a specific molecular arrangement. It should be noted that an average orientation angle of  $56^\circ$  was obtained previously for a thick ordered film of DiMe-PTCDI grown on a S-passivated GaAs substrate.<sup>53,54</sup>

**3.2. EP-PTCDI Desorption. 3.2.1. UPS Measurements.** The dependence of UPS spectra on the annealing temperature is shown in Figure 13. The first spectrum (the lower curve) corresponds to an EP-PTCDI multilayer grown at  $35^\circ\text{C}$ . The second curve was taken after annealing at  $175^\circ\text{C}$  for  $\sim 5$  min; it shows a rapid decrease of the peak centered at  $-2.7\text{ eV}$  characteristic of the multilayer. This disappears for temperatures higher than  $200^\circ\text{C}$  where the contribution of states close to the Fermi level starts to be seen. Previous TOF-DRS measurements<sup>21</sup> showed that the film was stable up to  $150^\circ\text{C}$  where the desorption of the multilayer started, and for sample temperatures higher than  $200^\circ\text{C}$  the multilayer has completely desorbed leaving the substrate/organic interface layer. If the remaining layer would be a monolayer of EP-PTCDI molecules,

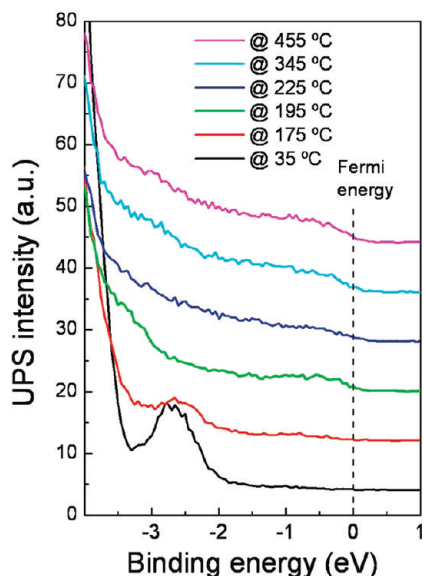


**Figure 13.** UPS spectra for a EP-PTCDI multilayer film grown at room temperature on Ag (111) after annealing at the temperatures indicated.

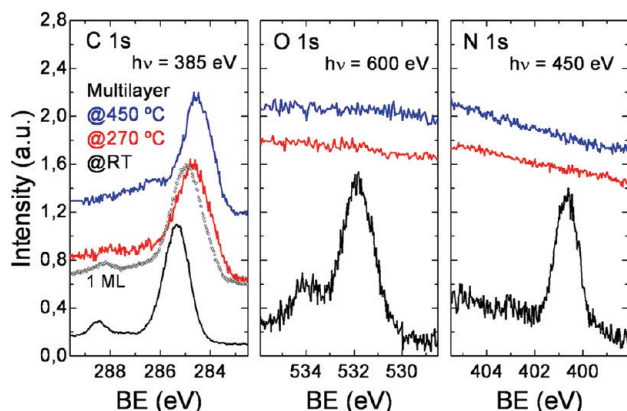


**Figure 14.** C 1s, O 1s, and N 1s XPS spectra of a multilayer film at room temperature, and annealed to 270 and 450 °C. The C 1s spectrum corresponding to one monolayer (1 ML) is also shown (open circles).

one would observe again the shoulder at about  $-3$  eV, and the peaks centered at  $-2.3$ ,  $-1.6$ , and  $-0.4$  eV as seen in Figure 6 for 1.3 ML, indicating that the remaining film does not correspond to the pristine ML.

**3.2.1. AES and XPS Measurements.** Auger electron spectroscopy (AES) experiments<sup>21</sup> taken at specific temperatures show essentially the same behavior of the TOF-DRS measurements, but in particular indicate depletion of oxygen above 170 °C. Thus from these measurements we would conclude that near 170 °C a second desorption process begins, where the ethyl-propyl chains and the oxygen atoms desorb, leaving some substrate regions clean and some containing components of the molecule, mainly the C and H species.

Here we performed XPS measurements to further explore these features. Figure 14 shows XPS spectra of the multilayer annealed to 270 and 450 °C. In agreement with the results just shown, for 270 °C the shape of the C1s XPS spectra is very similar to the spectra measured for 1 ML (although not the peak position), consistent with the fact that at this temperature the multilayer is absent<sup>21</sup> (a spectrum corresponding to the adsorption of 1 ML is also included in the figure). Only a very small amount of O is detected with XPS, while almost no trace of N

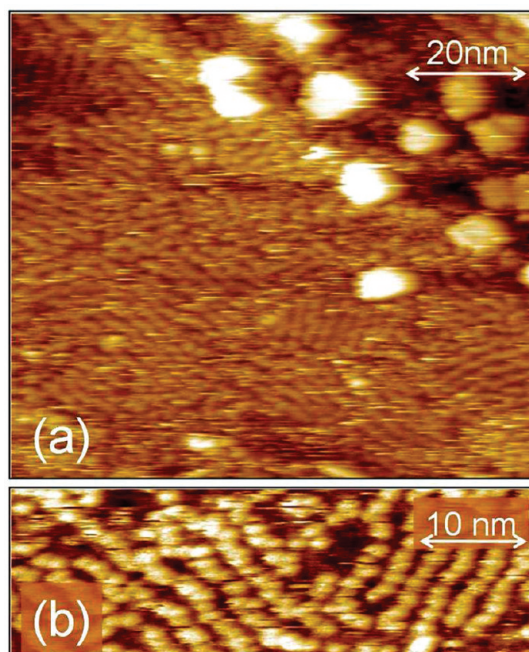


**Figure 15.** STM images of an EP-PTCDI multilayer annealed at 210 °C at (a) 2 V, 150 pA, and at (b) 2.5 V, 35 pA.

1s peak is observed indicating that the molecule dissociates leaving the perylene core, or at least part of its components, on the surface.

After heating the multilayer at 460 °C, the XPS shows that there are no N and O in the surface and only C remains (no information from H can be obtained by XPS).

**3.2.2. STM Measurements.** To complete the study of the desorption process we acquired STM images of the molecular arrangement on the surface for different annealing temperatures. After evaporation of the multilayer at room temperature, we annealed the sample up to 210 °C, the temperature at which the multilayer has mainly desorbed according to TOF-DRS experiments.<sup>21</sup> In Figure 15 we present two STM images taken after this first annealing. In panel a we can see some kind of striped short-range molecular ordering. We can also observe some very small islands of about 10 nm in diameter and 2 to 3 ML height. A more detailed STM image of the arrangement observed in panel a is shown in panel b. We can see that these “strips” are formed by small sections which have smaller dimensions than the entire EP-PTCDI molecule in agreement with the observation that the EP-PTCDI molecule has dissociated, as discussed in the previous section, and that there are parts of the substrate free of them.

We then increased the annealing temperature to 400 °C, which corresponds to the temperature at which all the multilayers have completely desorbed leaving only some components of the molecule (mainly formed by C and H atoms), without traces of O and N.

In Figure 16 we present two STM images of the surface after the second annealing. Panel a shows that a monolayer of smaller molecules remains in the surface with small areas free of them and without 3D island formation. The remaining molecules form some regions with no apparent order and large areas with well-ordered molecules forming a zigzag structure. In panel b we have scanned over the ordered area of the surface and we can see that the zigzag is formed of small bright spots that have the dimensions of the perylene core of the molecule. A scaled sketch of the perylene molecule shown in panel c of Figure 16 is

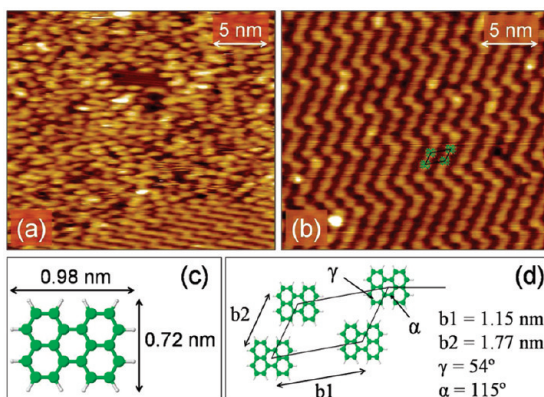


**Figure 16.** (a, b) STM images of an EP-PTCDI multilayer annealed at 400 °C (2.5 V, 25 pA and 2 V, 50 pA, respectively). (c) Sketch of a perylene molecule. (d) Proposed unit cell of the molecular arrangement observed in panel b.

included on the STM image shown in panel b, and a tentative structure of the arrangement of these molecules is presented in panel d. The exact orientation of each molecule with respect to the unit cell (the angle  $\alpha$ ) is difficult to ascertain in the present measurements but the size of the unit cell is correct.

These results, together with those obtained by the spectroscopic techniques, indicate that after annealing at 400 °C the molecule has dissociated losing the ethylpropyl end groups and the O and N atoms of the border of the molecule, leaving only the perylene core arranged on the surface like the unit cell shown in Figure 16d.

#### 4. Conclusions

In this work we have studied the adsorption kinetics, ordering, electronic structure, and thermal stability of thin EP-PTCDI films grown in Ag (111) by means of several surface science experimental (AFM, AES, NEXAFS, STM, UPS, and XPS) and theoretical (DFT) techniques.

For low coverages, STM imaging shows a fairly good organization of the molecules deposited at room temperature, with growth beginning at step edges, and completing a full ordered monolayer. Thus, at this stage, order is not hindered by the existence of the additional end groups of PTCDI molecules. For a few monolayers, the molecules are stacked parallel to the surface forming small 3D islands. For further depositions AFM imaging shows that the film continues to grow forming large 3D islands that do not completely coalesce.

UPS measurements show changes in the valence band in the monolayer to multilayer range indicating changes in molecule substrate interaction in agreement with the changes observed by the STM in the heights of the first and next layers.

NEXAFS indicates that at low coverages molecules lie almost flat (8°) on the surface in agreement with STM imaging. At high coverages, the multilayer is, however, disorganized.

Desorption of the molecular layer was studied up to a temperature of 455 °C. After annealing the sample at 200 °C, STM images show that most of the multilayer has disappeared, while for 400 °C a monolayer of other molecules, presumably the perylene core, remains in the surface forming large areas with ordered structures. Changes in electronic structure were followed by UPS and the composition was followed by XPS. XPS and previously reported AES and TOF-DRS measurements show that during the desorption process the last remaining monolayer loses not only part of the C atoms but all the N and O ones. The UPS measurements also indicate that the

original monolayer structure is not recovered. This agrees with a picture where the EP-PTCDI molecule loses the ethylpropyl end groups together with the O and N atoms of the PTCDI core, leaving only what appears to be a perylene core of the molecule.

DFT calculations show the configuration of an isolated molecule and confirm the stacking geometry of the first monolayer. It also provides information about the modification of the electronic density of states due to the interaction of the self-assembled monolayer and the Ag substrate.

**Acknowledgment.** We acknowledge support from ANPCyT (PME118, PICT 2003-14452, 2004-25959, 2005-33595, and 2006-715), CONICET (PIP 5248 and 112-200801-00958), U.N. Cuyo (06-C261 and 06-C266), Fundación Antorchas, and MinCyT (Argentina)-ECOS (France) Program (No. A07E01). We acknowledge support from the European Community, and we are grateful to Nicola Mahne and Angelo Giglia for their assistance during the experiments at Elettra.

#### References and Notes

- Theobald, J. A.; Oxtoby, N. S.; Phillips, M. A.; Champness, N. R.; Beton, P. H. *Nature* **2003**, *424*, 1029–1031.
- Graaf, H.; Schlettwein, D. *J. Appl. Phys.* **2006**, *100* (1–3), 126104.
- Ozcan, O.; Yukruk, F.; Akkaya, E. U.; Uner, D. *Appl. Catal. B* **2007**, *71*, 291–297.
- Bulovic, V.; Burrows, P. E.; Forrest, S. R. *Electroluminescence* **2000**, *64*, 255–306.
- Dodalapur, A. *Solid State Commun.* **1997**, *102*, 269–267.
- Horowitz, G. *J. Mater. Res.* **2004**, *19*, 1946–1962.
- Sun, S.-S.; Sariciftci, N. S. *Organic Photovoltaics: Mechanism, Materials and Devices*; CRC Press: Boca Raton, FL, 2005.
- Rost, C.; Karg, S.; Reiss, W.; Loi, M. A.; Murgia, M.; Muccini, M. *Synth. Met.* **2004**, *146*, 237–241.
- Temirov, R.; Soubatch, S.; Luican, A.; Tautz, F. S. *Nature* **2006**, *444*, 350–353.
- Chizhov, I.; Kahn, A.; Scoles, G. *J. Cryst. Growth* **2000**, *208*, 449–458.
- Balakrishnan, K.; Datar, A.; Naddo, T.; Huang, J.; Oitker, R.; Yen, M.; Zhao, J.; Zang, L. *J. Am. Chem. Soc.* **2006**, *128*, 7390–7398.
- Suemori, K.; Miyata, T.; Hiramoto, M.; Yokoyama, M. *Jpn. J. Appl. Phys.* **2004**, *43*, L1094–L1096.
- Weitz, R. T.; Amsharov, K.; Zschieschang, U.; Barrena Villas, E.; Goswami, D. K.; Burghard, M.; Dosch, H.; Jansen, M.; Kern, K.; Klauk, H. *J. Am. Chem. Soc.* **2008**, *130*, 4637–4645.
- Schmidtke, J. P.; Friend, R. H.; Kastler, M.; Müllen, K. *J. Chem. Phys.* **2006**, *124* (1–6), 174704.
- Burghard, M.; Fischer, C. M.; Roth, S.; Schlick, U.; Hanack, M. *Synth. Met.* **1996**, *76*, 241–244.
- Méndez, H.; Thurzo, I.; Zahn, D. R. T. *Phys. Rev. B* **2007**, *75* (1–14), 045321.
- Zahn, D. R. T.; Gavrila, G. N.; Salvan, G. *Chem. Rev.* **2007**, *107*, 1161–1232.
- Glöckler, K.; Seidel, C.; Soukopp, A.; Sokolowski, M.; Umbach, E.; Böhringer, M.; Berndt, R.; Schneider, W.-D. *Surf. Sci.* **1998**, *405*, 1–20.
- Nowakowski, R.; Seidel, C.; Fuchs, H. *Surf. Sci.* **2004**, *562*, 53–64.
- Seidel, C.; Schäfer, A. H.; Fuchs, H. *Surf. Sci.* **2000**, *459*, 310–322.
- Serkovic, L. N.; Sánchez, E. A.; Gayone, J. E.; Grizzi, O.; Esaulov, V. A. *Phys. Chem. Chem. Phys.* **2009**, *11*, 3849–3853.
- Private communication: Wiatrowsky, M. Department of Molecular Physics, University of Lodz, Poland.
- Serkovic Loli, L. N.; Gayone, J. E.; Sánchez, E. A.; Grizzi, O.; Esaulov, V. A. *Acta Microscopica*. In press.
- Soubiron, T.; Vaurette, F.; Nys, J. P.; Grandidier, B.; Wallart, X.; Stiévenard, D. *Surf. Sci.* **2005**, *581*, 178–188.
- Tautz, F. S. *Prog. Surf. Sci.* **2007**, *82*, 479–520.
- Gustafsson, J. B.; Zhang, H. M.; Johansson, L. S. O. *Phys. Rev. B* **2007**, *75* (1–17), 155414.
- Krause, B.; Dürr, A. C.; Schreiber, F.; Dosch, H.; Seeck, O. H. *J. Chem. Phys.* **2003**, *119*, 3429–3434.
- Henze, S. K. M.; Bauer, O.; Lee, T.-L.; Sokolowski, M.; Tautz, F. S. *Surf. Sci.* **2007**, *601*, 1566–1573.
- Swarbrick, J. C.; Ma, J.; Theobald, J. A.; Oxtoby, N. S.; O'Shea, J. N.; Champness, N. R.; Beton, P. H. *J. Phys. Chem. B* **2005**, *109*, 12167–12174.

- (30) Giglia, A.; Mahne, N.; De Luisa, A.; Doyle, B.; Borgatti, F.; Pedio, M.; Pasquali, L.; Naletto, G.; Pelizzo, M. G.; Tondello, G. *Not. Neutroni Luce Sincrotrone* **2007**, *12*, 8–19.
- (31) Pasquali, L.; Terzi, F.; Seeber, R.; Doyle, B.; Nannarone, S. *J. Chem. Phys.* **2008**, *128* (1–10), 134711.
- (32) Lamont, C. L. A.; Wilkes, J. *Langmuir* **1999**, *15*, 2037–2042.
- (33) Yeh, J. J.; Lindau, I. *Atomic Calculation of Photoionization Cross-Sections and Asymmetry Parameters*; Gordon and Breach Science Publishers: New York, 1993.
- (34) Im Langenbroich 20-D-52428 Juelich, Germany <http://www.mateck.de/>.
- (35) ChemiePark, Areal A Sensientstrasse 3 D-06766 Wolfen, Germany.
- (36) Payne, M. C.; Teter, M. P.; Allen, D. C.; Joannopoulos, J. D. *Rev. Mod. Phys.* **1992**, *64*, 1045–1097.
- (37) Kresse, G.; Furthmüller, J. *Phys. Rev. B* **1996**, *54*, 11169–11186.
- (38) Vanderbilt, D. *Phys. Rev. B* **1990**, *41*, 7892–7895.
- (39) Kresse, G.; Hafner, J. *J. Phys.: Condens. Matter* **1994**, *6*, 8245–8257.
- (40) Perdew, J. P.; Wang, Y. *Phys. Rev. B* **1992**, *45*, 13244–13249.
- (41) Monkhorst, H. J.; Pack, J. D. *Phys. Rev. B* **1976**, *13*, 5188–5192.
- (42) Methfessel, M.; Paxton, A. T. *Phys. Rev. B* **1989**, *40*, 3616–3621.
- (43) Tersoff, J.; Hamann, D. R. *Phys. Rev. B* **1985**, *31*, 805–813.
- (44) Hofer, W. A.; Redinger, J. *Surf. Sci.* **2000**, *447*, 51–61.
- (45) Duham, S.; Gerlach, A.; Salzmann, I.; Bröker, B.; Johnson, R. L.; Schreiber, F.; Koch, N. *Org. Electron.* **2008**, *9*, 111–118.
- (46) Zou, Y.; Kilian, L.; Schöll, A.; Schmidt, Th.; Fink, R.; Umbach, E. *Surf. Sci.* **2006**, *600*, 1240–1251.
- (47) Kampen, T. U.; Das, A.; Park, S.; Hoyer, W.; Zahn, D. R. T. *Appl. Surf. Sci.* **2004**, *234*, 333–340.
- (48) Schöll, A.; Zou, Y.; Huebner, D.; Urquhart, S. G.; Schmidt, Th.; Fink, R.; Umbach, E. *J. Chem. Phys.* **2005**, *123* (1–15), 044509.
- (49) Tabaroski, J.; Väterlein, P.; Dietz, H.; Zimmermann, U.; Umbach, E. *J. Electron Spectrosc. Relat. Phenom.* **1995**, *75*, 129–147.
- (50) Gustafsson, J. B.; Moons, E.; Widstrand, S. M.; Gurnett, M.; Johansson, L. S. O. *Surf. Sci.* **2004**, *572*, 32–42.
- (51) Hänel, K.; Söhnchen, S.; Lukas, S.; Beernink, G.; Birkner, A.; Strunskus, T.; Witte, G.; Wöll, Ch. *J. Mater. Res.* **2004**, *19*, 2049–2056.
- (52) Stöhr, J. *NEXAFS Spectroscopy*; Springer-Verlag: Berlin, Germany, 1992.
- (53) Friedrich, M.; Gavrila, G.; Himcinschi, C.; Kampen, T. U.; Yu Kobitski, A.; Méndez, H.; Savan, G.; Cerrilló, I.; Méndez, J.; Nicoara, N.; Baró, A. M.; Zahn, D. R. T. *J. Phys.: Condens. Matter* **2003**, *15*, S2699–S2718.
- (54) Gavrila, G. N.; Mendez, H.; Kampen, T. U.; Zahn, D. R. T.; Vyalikh, D. V.; Braun, W. *Appl. Phys. Lett.* **2004**, *85* (1–3), 4657.

JP9051769